Total Variation Based Convex Filters for Medical Imaging

Stephen L. Keeling*

Abstract. Several variational based diffusion filters are applied to measured magnetic resonance images, and on this basis are evaluated for their suitability to medical imaging. In particular, a specific total variation based filter with a convex variational penalty function is introduced here for the enhancement of *edge*, *flat*, and *grey* image scales. In general, results reveal that convex total variation based filters can be implemented to perform very well to enhance the visual clarity of medical images. As a result, further support is provided to establish such methods for medical applications.

1 Introduction.

A natural way of selecting from possible enhancements of a measured image is by minimizing an appropriate cost. This paper is concerned with the qualitative evaluation of certain variational based filters for their suitability to medical imaging. Specifically, for an unfiltered image u_0 defined on an image domain P let u be a filtered image defined as a minimizer for the functional:

$$J(u) = \int_P \phi(|\nabla u|)dx + \frac{\mu}{2}\int_P |u_0 - u|^2 dx \tag{1.1}$$

for which the necessary optimality condition is expressed in the steady state for the following descent minimization method:

$$\partial_t u = \nabla\cdot(g(|\nabla u|)\nabla u)+\mu(u_0-u), \quad P\times[0,\infty), \qquad u_n = 0, \quad \partial P\times[0,\infty), \qquad u(0) = u_0, \quad P. \tag{1.2}$$

Here, the variational penalty function ϕ gives the diffusivity $g(s) = \phi'(s)/s$. Such filters are also implemented by nullifying μ and alternatively choosing a final diffusion time as a regularization parameter. In either case, this diffusion can be seen as a natural filtering process in which undesirable image features are dissipated while desirable features are either preserved or accentuated.

These filters are usefully classified according to whether the variational penalty function ϕ is convex ($\phi'' > 0$), concave ($\phi'' < 0$), or mixed in the sign of ϕ''. This classification is revealing since convexity has a smoothing effect on the filtered image, while concavity is necessary for edge sharpening [1]. On the one extreme of convexity is classical Gaussian filtering which is still used [2] in spite of its well known excessive smoothing properties [3]. On the other extreme of concavity is balanced-forward-backward (BFB) diffusion filtering [4] which provides multiscale edge enhancement over a wide range of slopes, which nevertheless must be modulated to avoid amplification of noisy gradients. Perona-Malik filtering [5] involves combining a zone of convexity with a zone of concavity, but such filters are necessarily tuned to enhance a narrow range of edge slopes; otherwise, edges are either blurred or staircased [4]. At the interface between convexity and concavity is total variation (TV) filtering [6] for which $\phi'' = 0$. TV filtering is known for its excellent reconstruction of apparently piecewise constant or *blocky* images. However, while TV filtering provides excellent edge preservation and excellent smoothing of flat regions, it suffers from a well known staircasing effect in regions with gradual image variations [3]. In other words, TV filtering treats *edge* and *flat* scale gradients well, but not *grey* scale gradients; therefore, edge-flat-grey (EFG) scale filtering [7] was developed by making ϕ'' strictly positive

*Institut für Mathematik, Karl-Franzens-Universität Graz, Heinrichstraße 36, 8010 Graz, Austria; email: Stephen.Keeling@kfunigraz.ac.at; tel: +43–316–380–5156; fax: +43–316–380–9815. Support from the Fonds zur Förderung der wissenschaftliche Forschung under SFB F003, "Optimierung und Kontrolle".

for grey scales. Finally, Gauss-TV filtering [8] can be used to treat images as consisting of only grey and edge scale gradients.

The suitability of a given filter for medical imaging in particular depends naturally upon the specific goal of interest, and two classes of objectives can be identified. On the one hand, it may be necessary to remove image noise without altering any underlying image details. Such denoising can be required, for example, prior to further quantitative image processing which can be particularly susceptible to measurement error; consider, e.g., diffusion tensor imaging [9]. On the other hand, it may be necessary to enhance specific features qualitatively by significantly modifying the image at the expence of quantitative accuracy. For example, accentuation of edges [4] or of fibers [3] can greatly facilitate a detailed visual examination of (potentially pathological) sites containing such features. Also, a reduction in the image histogram spread, or rather an increased flattening of homogeneous image regions, can greatly facilitate the segmentation of an image into its component tissue types. In this paper, several filters are applied to measured noisy magnetic resonance images (MRIs), and the results are discussed primarily with respect to the goal of denoising. However, since some of these filters apparently provide good edge enhancement or good segmentation preconditioning, these goals are discussed as well. It is apparent from the results that convex total variation based filters can be implemented to perform very well for the medical imaging objectives explained here. As a result, further support is provided to establish such methods for medical applications.

2 Review of Filters.

Six parameterized diffusion filters are listed in Table 1 along with related functions considered in this paper. The diffusion properties of these filters can be further elucidated by the orthogonal decomposition of Eqn. (1.2) as follows [10]:

$$\partial_t u = \phi''(|\nabla u|)u_{\nu\nu} + g(|\nabla u|)(\nabla^2 u - u_{\nu\nu}) + \mu(u_0 - u) \tag{2.1}$$

where $u_{\nu\nu}$ is the second derivative of u in the direction of ∇u. Thus, with respect to level sets of u, the first term captures normal diffusion and the second captures tangential diffusion. Therefore, diffusion normal to level sets of u is forward where $\phi'' > 0$ and it is backward where $\phi'' < 0$. Note that the filters are listed in Table 1 in the order of increasing dissipativeness in the normal direction. On the other hand, tangential diffusion is forward in every case since the diffusivity $g(s) > 0$. Because of this directional dependence of the diffusion, it is said to be *anisotropic*. On the other hand, diffusion processes are sometimes called anisotropic when g is a diffusion tensor [3] and then even the flux $g\nabla u$ may not be parallel to ∇u. In this paper, only scalar diffusivities are considered.

The balanced-forward-backward (BFB) diffusion filter [4] provides multiscale edge enhancement by balancing backward diffusion normal to level sets with forward diffusion tangent to level sets:

$$\frac{\phi''(s)}{g(s)} = -\frac{s}{\kappa + s} \to -1, \qquad \kappa \to 0. \tag{2.2}$$

Thus, as seen in Eqn. (2.1), the normal and tangential diffusion coefficients are balanced at all scales as $\kappa \to 0$. To avoid the enhancement of noisy gradients, a $\kappa > 0$ can be used so that the filter follows the TV model for smaller gradients and the BFB model for larger gradients.

As seen from Eqn. (2.1) and Table 1, the Perona-Malik (PM) diffusion filter [5] provides diffusion normal to level sets of u which is forward where $|\nabla u| < \lambda$ and backward where $|\nabla u| > \lambda$. This construction is motivated by the fact that one-dimensional edge enhancing diffusion requires the following conditions at an edge:

$$\begin{aligned} \partial_t u_\nu &= \phi'' u_{\nu\nu\nu} + \mu(u_0 - u)_\nu \;>\; 0 \\ \partial_t u_{\nu\nu\nu} &= 3\phi''' u_{\nu\nu\nu}^2 + \phi'' u_{\nu\nu\nu\nu\nu} + \mu(u_0 - u)_{\nu\nu\nu} \;<\; 0. \end{aligned} \tag{2.3}$$

Filter	$\phi(s)$	$g(s) = \dfrac{\phi'(s)}{s}$	$\phi''(s)$
1. BFB	$\log(\kappa + s)$	$\dfrac{1}{s(\kappa+s)}$	$-\dfrac{1}{(\kappa+s)^2}$
2. PM	$\lambda^2\left(1-\exp\left[-\frac{1}{2}\left(\frac{s}{\lambda}\right)^2\right]\right)$	$\exp\left[-\frac{1}{2}\left(\frac{s}{\lambda}\right)^2\right]$	$\dfrac{1-\left(\frac{s}{\lambda}\right)^2}{\exp\left[\frac{1}{2}\left(\frac{s}{\lambda}\right)^2\right]}$
3. TV	s	$\dfrac{1}{s}$	0
4. EFG	$\begin{cases} \int_0^s e^{-q(\sigma)^2}d\sigma & 0\le s\le\gamma \\ s-\gamma+\int_0^\gamma e^{-q(\sigma)^2}d\sigma & s\ge\gamma \end{cases}$ $q(s)=1-\left(\frac{s}{\gamma}\right)^2$	$\begin{cases} \frac{1}{s}e^{-q(s)^2} & 0\le s\le\gamma \\ \frac{1}{s} & s\ge\gamma \end{cases}$	$\begin{cases} \frac{4s}{\gamma^2}q(s)e^{-q(s)^2} & 0\le s\le\gamma \\ 0 & s\ge\gamma \end{cases}$
5. Gauss-TV	$\begin{cases} \frac{s^2}{2} & 0\le s\le\delta \\ \delta s-\frac{\delta^2}{2} & s\ge\delta \end{cases}$	$\begin{cases} 1 & 0\le s\le\delta \\ \frac{\delta}{s} & s\ge\delta \end{cases}$	$\begin{cases} 1 & 0\le s\le\delta \\ 0 & s\ge\delta \end{cases}$
6. Gaussian	$\dfrac{s^2}{2}$	1	1

Table 1: Parameterized filter variational penalty functions $\phi(s)$ and related functions discussed within the text.

Here, Eqn. (2.1) is used along with the edge conditions that odd normal derivatives alternate in sign while even normal derivatives vanish. The first condition in Eqn. (2.3) provides that u_ν increases at edges and the second condition provides that $\partial_t u_\nu$ is locally maximal in the normal direction. These conditions require roughly that $\phi'' < 0$ and $\phi''' < 0$. Thus, with PM filtering, edges are only enhanced for gradient magnitudes in a narrow range just inside the concavity zone of ϕ. Otherwise, weaker slopes are blurred and stronger slopes are staircased. As a result, PM filtered images exhibit strongly flattened regions separated by jumps at positions tuned to the value of λ [4].

Total variation (TV) filtering [6] is at the interface between convexity and concavity where $\phi'' = 0$. Hence, according to Eqn. (2.1), TV filtering provides neither forward nor backward diffusion normal to level sets. Thus, edges are neither sharpened nor smoothed, but rather *preserved* during diffusion filtering. On the other hand, the pure tangential diffusion effectively smoothes flat regions of an image. This combination of edge preservation and flat region smoothing gives TV filtering an excellent performance for apparently piecewise constant images. However, as indicated for instance in Eqn. (2.3), the presence of the reaction term, $\mu(u_0 - u)$, can contribute to staircasing in regions with gradual image variations [11].

Thus, edge-flat-grey (EFG) scale filtering [7] was developed by making ϕ'' strictly positive for gradient magnitudes corresponding to gradual image variations, i.e., for grey scales between the flat and the edge scales. In this paper, the novel EFG function shown in Table 1 is introduced as a smooth variational penalty function meeting the conditions set forth in [7] while providing excellent edge-flat-grey scale filtering. For simplicity, suppose $\gamma = 1$ and observe that the EFG penalty function takes the form on the interval $[0, 1]$:

$$\phi'(s) = e^{-(1-s^2)^2} = s^{p(s)} - 1 \quad \text{with} \quad p(s) = 1 + \frac{(1-s^2)^2}{\log(1/s)}. \tag{2.4}$$

Thus, the EFG penalty corresponds roughly to an L_p penalty on $|\nabla u|$ where p varies as shown in the left plot of Fig. 1. Also, shown on the right in Fig. 1 is a plot of $\phi''(s)$ on the interval

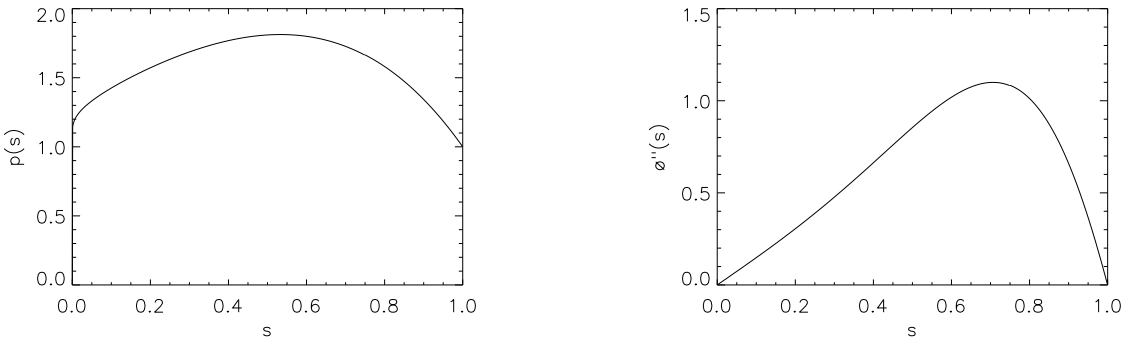

Figure 1: p from Eqn. (2.4) and ϕ'' in Eqn. (2.1).

$[0, 1]$. Note further that $p(0) = p(1) = 1$ and that $\phi'''(s)$ is bounded. In light of Eqn. (2.1), the plot of $\phi''(s)$ illustrates that diffusion normal to level sets of u is strictly positive for a range of gradient magnitudes, but drops to zero for sufficiently large and for vanishing gradients.

As demonstrated in the computational results, the EFG filter treats small slope regions as consisting of flat scale gradients and therefore flattens such regions. As indicated in the Introduction, the effect can be used to advantage for segmentation preconditioning, but the visual consequence is a loss of a natural three-dimensional appearance. On the other hand, it is shown here that a more natural appearance can be created for medical images in particular by using Gauss-TV filtering to treat images as consisting of essentially only edge and grey scales. Note from Table 1 that the diffusivity $g(s)$ for Gauss-TV filtering has the same bell shape as that of the PM diffusivity, but the filter performs much differently; see also [8]. The initial portion of this diffusivity corresponds to Gaussian filtering and, as discussed in the next paragraph,

it therefore provides isotropic dissipation for gradients with $|\nabla u| < \gamma$. The later portion of this diffusivity corresponds to TV filtering and, as discussed above, it therefore provides edge preservation for gradients with $|\nabla u| > \gamma$.

Finally, with Gaussian filtering [12] [13] [2], both the normal and tangential diffusion coefficients in Eqn. (2.1) are equal to one, and the resulting linear heat equation provides isotropic dissipation for all gradient magnitudes. In some settings, Gauss filtered images are computed pixelwise merely by performing a single weighted average of values in neighboring pixels [2]; however, this computation corresponds to a single explicit step for advancing the discretized linear heat equation. Naturally, this classical smoothing filter can reduce noise, but its very strong forward diffusion leads to a rapid loss of image details.

3 Numerical Methods.

The filters given in Table 1 were implemented numerically for this study as follows. In brief, the spatial discretization of Eqn. (1.2) is accomplished with finite differences and the temporal discretization is accomplished with implicit time stepping. All cells are assumed to have unit aspect ratios and width h. For planar images, Cartesian central differences are used to discretize the diffusion operator at the cell centroid $(x_i, y_j) = ((i - \frac{1}{2})h, (j - \frac{1}{2})h)$, where $1 \le i, j \le N$, as follows:

$$\begin{aligned} h^2[\nabla \cdot (g(|\nabla U|)\nabla U)]_{i,j} &= g(|\nabla U|_{i+\frac{1}{2},j})\,[U_{i+1,j} - U_{i,j}] - g(|\nabla U|_{i-\frac{1}{2},j})\,[U_{i,j} - U_{i-1,j}] \\ &+ g(|\nabla U|_{i,j+\frac{1}{2}})\,[U_{i,j+1} - U_{i,j}] - g(|\nabla U|_{i,j-\frac{1}{2}})\,[U_{i,j} - U_{i,j-1}]\,. \end{aligned} \tag{3.1}$$

Here, the notation $U(x_i, y_j, t) = U_{i,j}(t)$ is used for an approximation to $u(x_i, y_j, t)$, and $U^n_{i,j}$ is used to denote an approximation to $u(x_i, y_j, t^n)$ at the nth time level $t^n = n\tau$. Also, $\bar{U}(t)$ and $\bar{U}^n$ represent the vectors $\{U_{i,j}(t)\}$ and $\{U^n_{i,j}\}$. For diffusivity computations, the gradient terms $|\nabla U|$ are computed at cell interfaces as follows:

$$2|\nabla U|_{i\pm\frac{1}{2},j} = |\nabla U|_{i\pm\frac{1}{2},j+\frac{1}{2}} + |\nabla U|_{i\pm\frac{1}{2},j-\frac{1}{2}}, \quad 2|\nabla U|_{i,j\pm\frac{l}{2}} = |\nabla U|_{i+\frac{1}{2},j\pm\frac{1}{2}} + |\nabla U|_{i-\frac{1}{2},j\pm\frac{1}{2}}, \tag{3.2}$$

where:

$$2[h|\nabla U|_{i+\frac{k}{2},j+\frac{l}{2}}]^2 = |U_{i+k,j+l} - U_{i,j}|^2 + |U_{i+k,j} - U_{i,j+l}|^2, \quad k, l = \pm 1. \tag{3.3}$$

Here, values of U with out-of-range indices are understood equal to their reflections across the image boundary, and values of g at cell interfaces on the boundary are understood to be zero. As a result of computing the discrete diffusion operator at the boundary in this way, natural no-flux boundary conditions are implemented implicitly. Also, the discrete diffusion can be written as the product $h^{-2}G(\bar{U})\bar{U}$ for a symmetric matrix G. Assume that the unbounded diffusivities are actually computed as $g(\max\{s, \varepsilon\})$ to avoid division by zero. Here, ε is not viewed as an additional parameter as it is simply chosen near machine zero or small enough for results to be insensitive to its variation. Also, the above Cartesian discretizations are used to provide sufficient coupling among cells as opposed to that associated, for instance, with diagonal discretizations as discussed in [4]. Note that these spatial discretizations can be defined similarly in other spatial dimensions.

Now, with $\bar{U}_0$ denoting the initial image values, the semidiscrete formulation of the filter is $\bar{U}' = h^{-2}G(\bar{U})\bar{U}, \;\; \bar{U}(0) = \bar{U}_0$. Then, a fully discrete formulation is obtained with the following implicit time stepping:

$$\left[I - \rho G(\bar{U}^n)\right]\bar{U}^{n+1} = \bar{U}^n, \qquad \bar{U}^0 = \bar{U}_0 \tag{3.4}$$

where $\rho = \tau h^{-2}$. These time stepping equations are solved only approximately, using just a few iterations of a Jacobi preconditioned conjugate gradient method [14].

4 Computational Results.

All the computations reported in this section were performed using the IDL[†] (Interactive Data Language) system. While image magnifications are used to demonstrate image features in hard copy form, it should be emphasized that these features are much more conspicuous on a high resolution monitor. In every example, $N = 256$ and $h = 1$; hence, for time stepping $\rho = \tau$. Also, time stepping is performed with two conjugate gradient iterations after the initial gradient step.

Next, the following parameters were readily determined empirically and used for the respective methods to achieve apparently best quality results. For BFB: $\tau = 0.001$, $n = 5$, $\kappa = 0.5$, and $\mu = 0.0$. For PM: $\tau = 0.4$, $n = 5$, $\lambda = 0.015$, and $\mu = 0.0$. For TV without a reaction term: $\tau = 0.002$, $n = 5$, and $\mu = 0.0$. For TV with a reaction term: $\tau = 0.007$, $n = 5$, and $\mu = \tau^{-1}$. For EFG: $\tau = 0.5$, $\gamma = 0.05$, $n = 5$, and $\mu = \tau^{-1}$. For Gauss-TV: $\tau = 0.7$, $\delta = 0.05$, $n = 5$, and $\mu = \tau^{-1}$.

Finally, note that two classical filters were implemented as follows [2]. Median filtering was implemented by replacing $U^0_{i,j}$ with the median value from $\{U^0_{i+k,j+l} : |k|, |l| \leq 1\}$. Also, Gauss filtering was implemented by replacing $U^0_{i,j}$ with the weighted average of values in neighboring pixels which corresponds to the explicit discretization of the heat equation:

$$\begin{aligned}\frac{U^1_{i,j} - U^0_{i,j}}{\tau} &= \frac{1}{h}\left\{\left[\frac{U^0_{i+1,j} - U^0_{i,j}}{h} - \frac{U^0_{i,j} - U^0_{i-1,j}}{h}\right] + \left[\frac{U^0_{i,j+1} - U^0_{i,j}}{h} - \frac{U^0_{i,j} - U^0_{i,j-1}}{h}\right]\right\} \\ &+ \frac{1}{\sqrt{2}h}\left\{\left[\frac{U^0_{i+1,j+1} - U^0_{i,j}}{\sqrt{2}h} - \frac{U^0_{i,j} - U^0_{i-1,j-1}}{\sqrt{2}h}\right] + \left[\frac{U^0_{i+1,j-1} - U^0_{i,j}}{\sqrt{2}h} - \frac{U^0_{i,j} - U^0_{i-1,j+1}}{\sqrt{2}h}\right]\right\}\end{aligned} \tag{4.1}$$

with $8\tau = h^2$. Because of the associated edge preserving properties, median filtered results are shown first before the results for the concave filters in Table 1. On the other hand, because of the associated dissipative properties, Gauss filtered results are shown last after the results for the convex filters. Results for all the filters are summarized in Table 2.

Figures 2 and 3 show the results of the aforementioned filters when applied to the noisy magnetic resonance images shown in Figs. 2a and 3a, respectively. Specifically, the image shown in Fig. 2a is an MRI of an *in vitro* atherosclerotic vessel, and the image shown in Fig. 3a is an MRI of the abdomen including a blood pooling contrast agent. In both figures, the right column of images contains magnifications from the corresponding images in the left column. In Fig. 2, the zone of magnification is indicated by the black boundary in Fig. 2a, while in Fig. 3, the zones of magnification are indicated by the white boundaries in Fig. 3a. Note that since the background of the MRI in Fig. 2 is simply the signal from the fluid bath in which the vessel is suspended, this image provides a good test for a filter's treatment of regions which should be flat. On the other hand, the MRI in Fig. 3 contains a great variety of gradient scales, including edges, rounded structures, pointed structures, flat regions, and regions of gradual variations; thus, this image provides a good test for a filter's treatment of images of *in vivo* tissues.

From Figs. 2b and 2e and Figs. 3b and 3e, note that the median filter does preserve the stronger edges but it imparts a *sawtooth* appearance to diagonally oriented edges. Specifically, this sawtooth appearance is evident in nearly every edge in Fig. 2e, and in Fig. 3e especially around the boundary of the spleen shown in the upper right. Otherwise, the filter smoothes details associated with insufficiently large gradients. Specifically, there is a conspicuous loss of details in the pelvic region shown in the lower left of Fig. 3e. Furthermore, this smoothing of gradients below a certain threshold creates a *splotchy* background in the flat region of Figs. 2b and 2e corresponding to the fluid bath. Since the median filter strongly changes the shape of edges either by sawtoothing or by smoothing, it is not well suited to either edge enhancement

[†]See `http://www.rsinc.com/idl/index.cfm`.

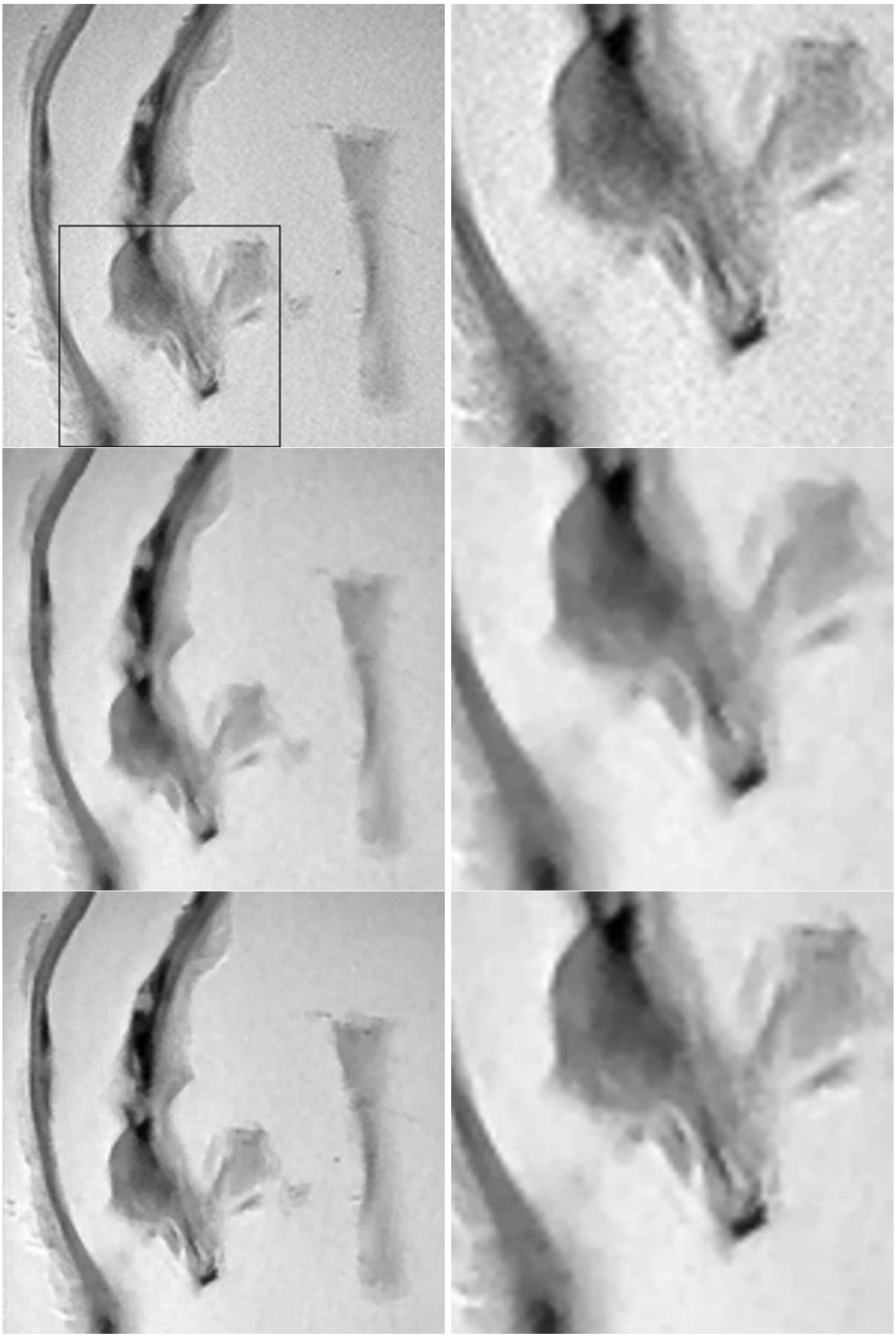

Figure 2: (a) TOP LEFT: an unfiltered magnetic resonance image u_0 of an atherosclerotic vessel, (b) MIDDLE LEFT: u_0 after median filtering, (c) BOTTOM LEFT: u_0 after BFB filtering, and (d – f) RIGHT COLUMN: magnifications from images (a – c), respectively.

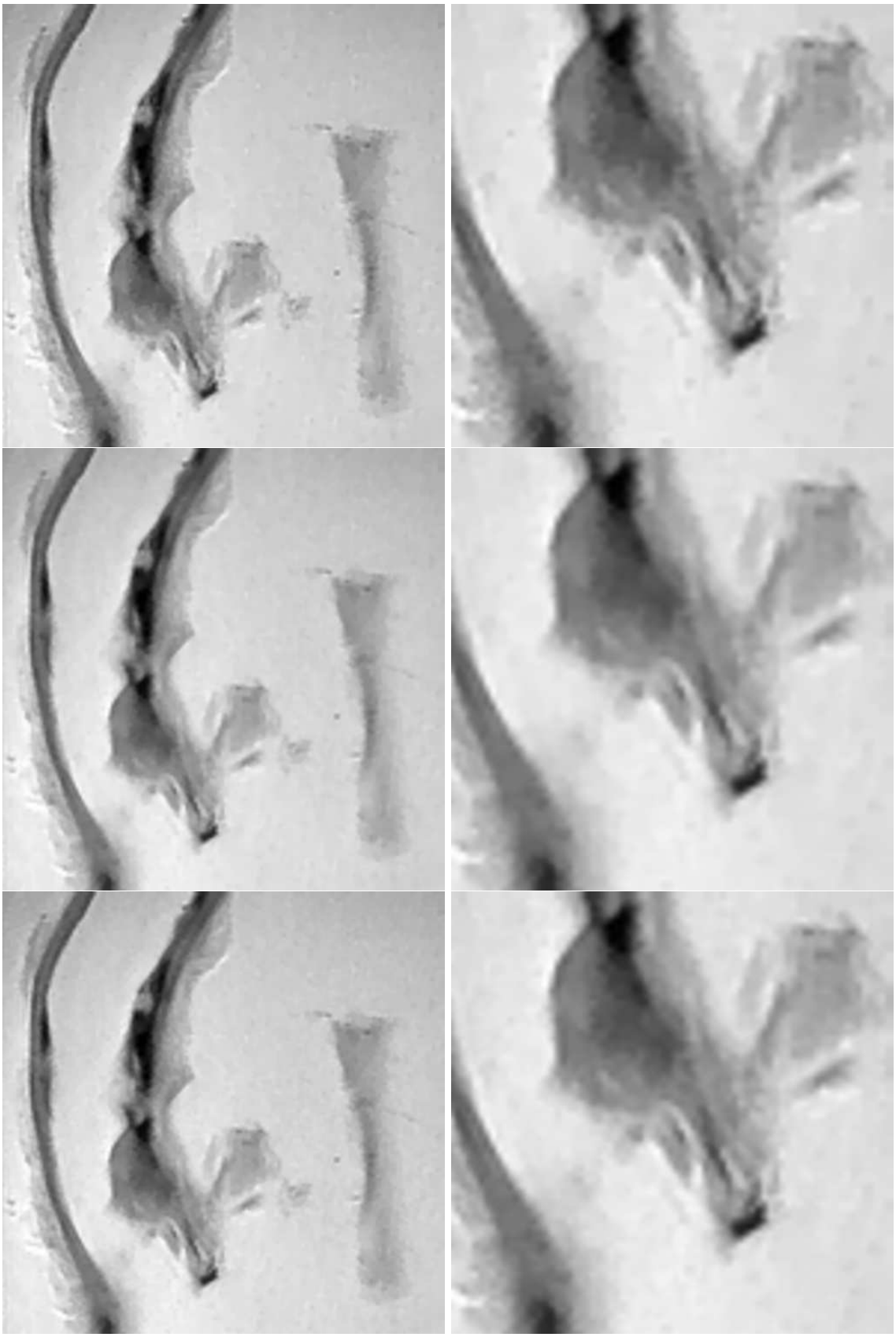

Figure 2: (g) TOP LEFT: u_0 after PM filtering, (h) MIDDLE LEFT: u_0 after TV filtering without reaction term, (i) BOTTOM LEFT: u_0 after TV filtering with reaction term, and (j – l) RIGHT COLUMN: magnifications from images (g – i), respectively.

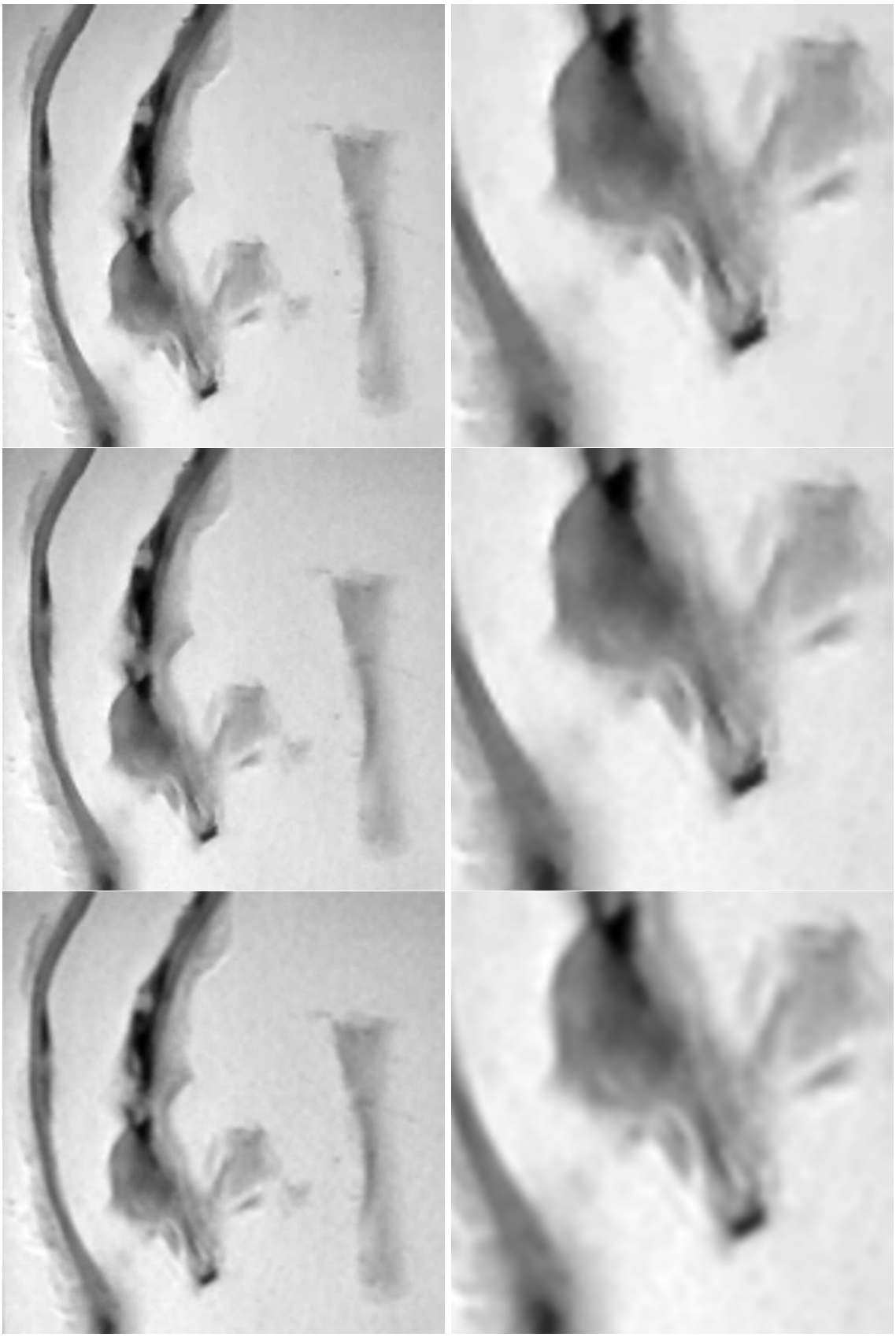

Figure 2: (m) TOP LEFT: u_0 after EFG filtering, (n) MIDDLE LEFT: u_0 after Gauss-TV filtering, (o) BOTTOM LEFT: u_0 after Gauss filtering, and (p – r) RIGHT COLUMN: magnifications from images (m – o), respectively.

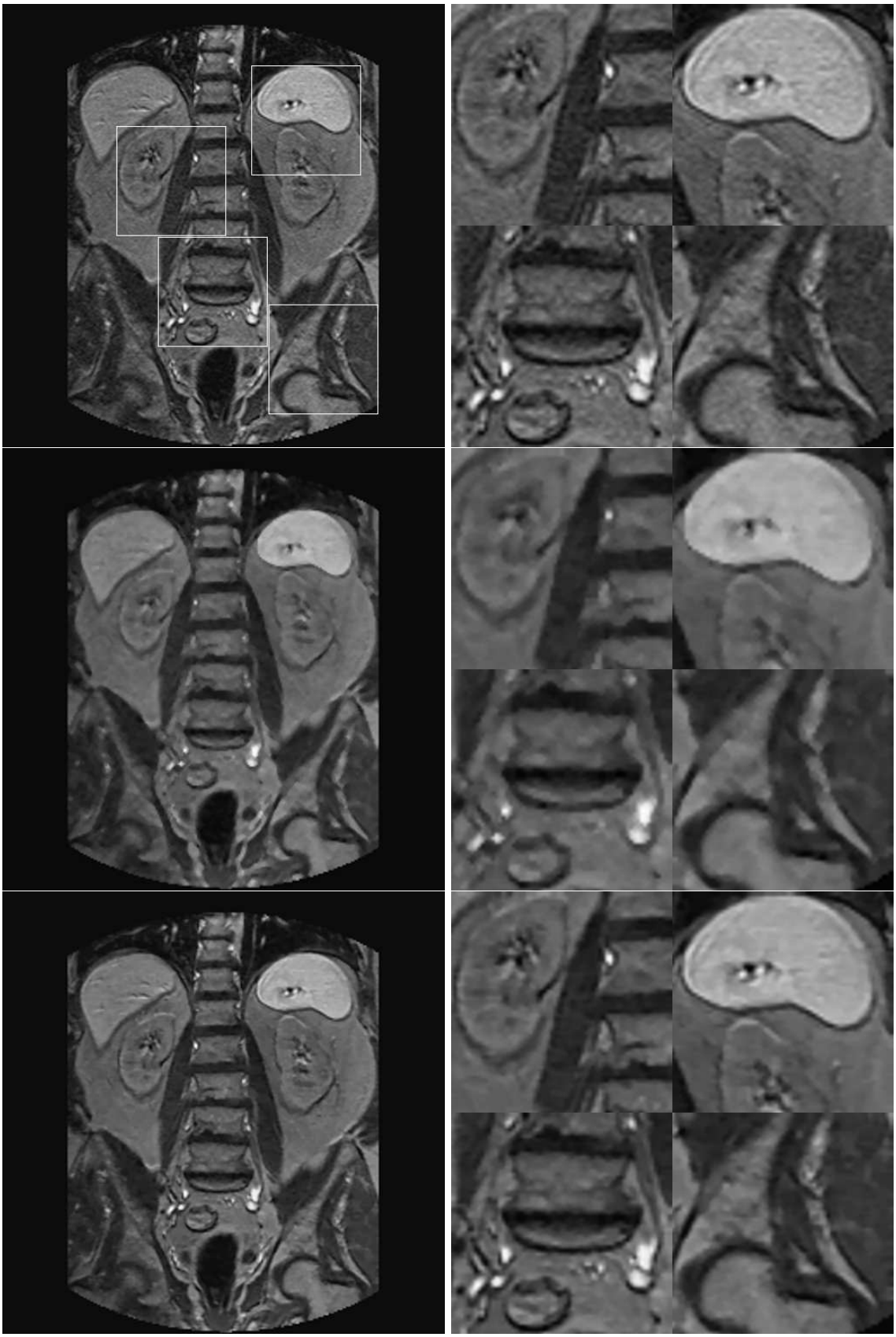

Figure 3: (a) TOP LEFT: an unfiltered magnetic resonance image u_0 of the abdomen, (b) MIDDLE LEFT: u_0 after median filtering, (c) BOTTOM LEFT: u_0 after BFB filtering, and (d – f) RIGHT COLUMN: magnifications from images (a – c), respectively.

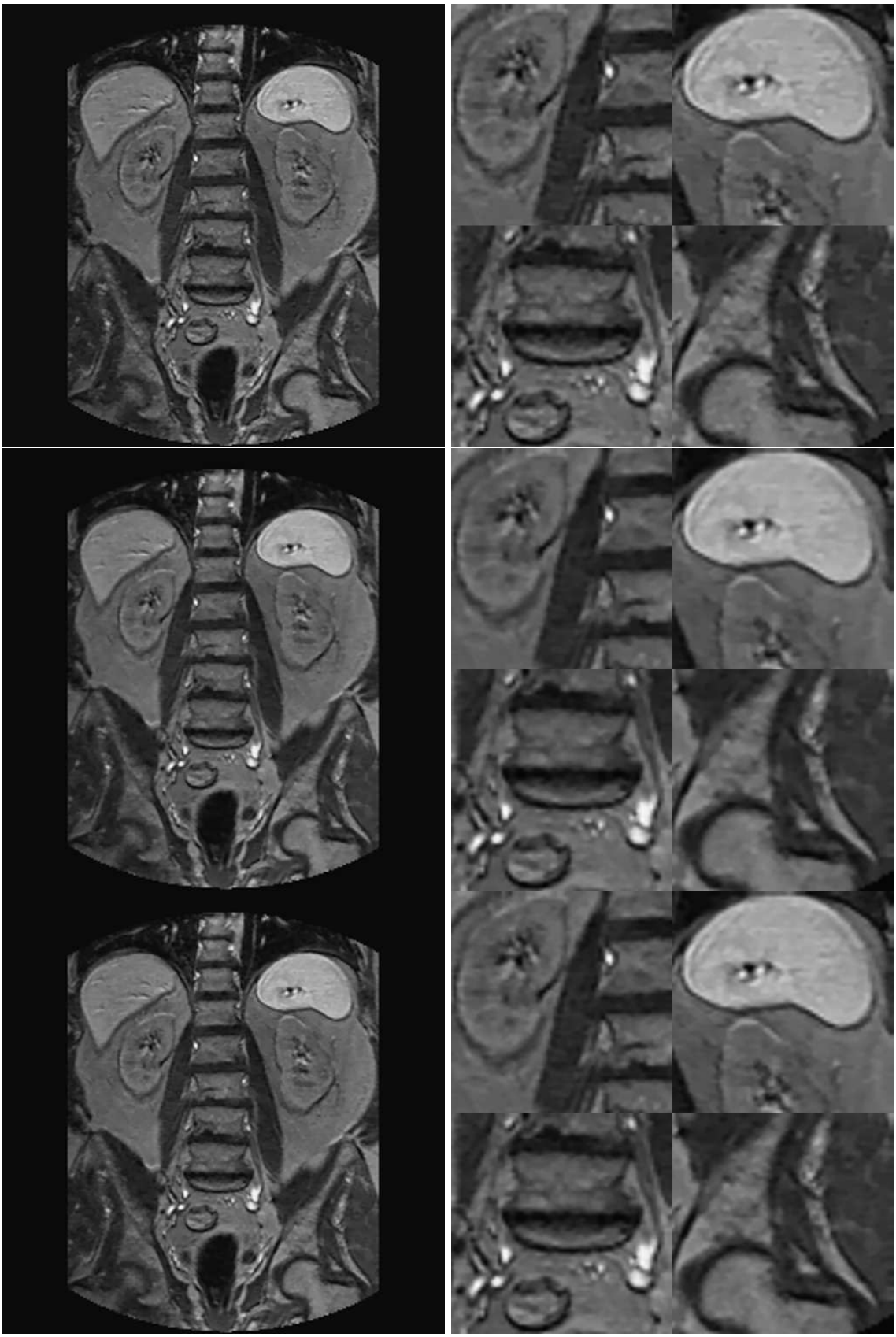

Figure 3: (g) TOP LEFT: u_0 after PM filtering, (h) MIDDLE LEFT: u_0 after TV filtering without reaction term, (i) BOTTOM LEFT: u_0 after TV filtering with reaction term, and (j – l) RIGHT COLUMN: magnifications from images (g – i), respectively.

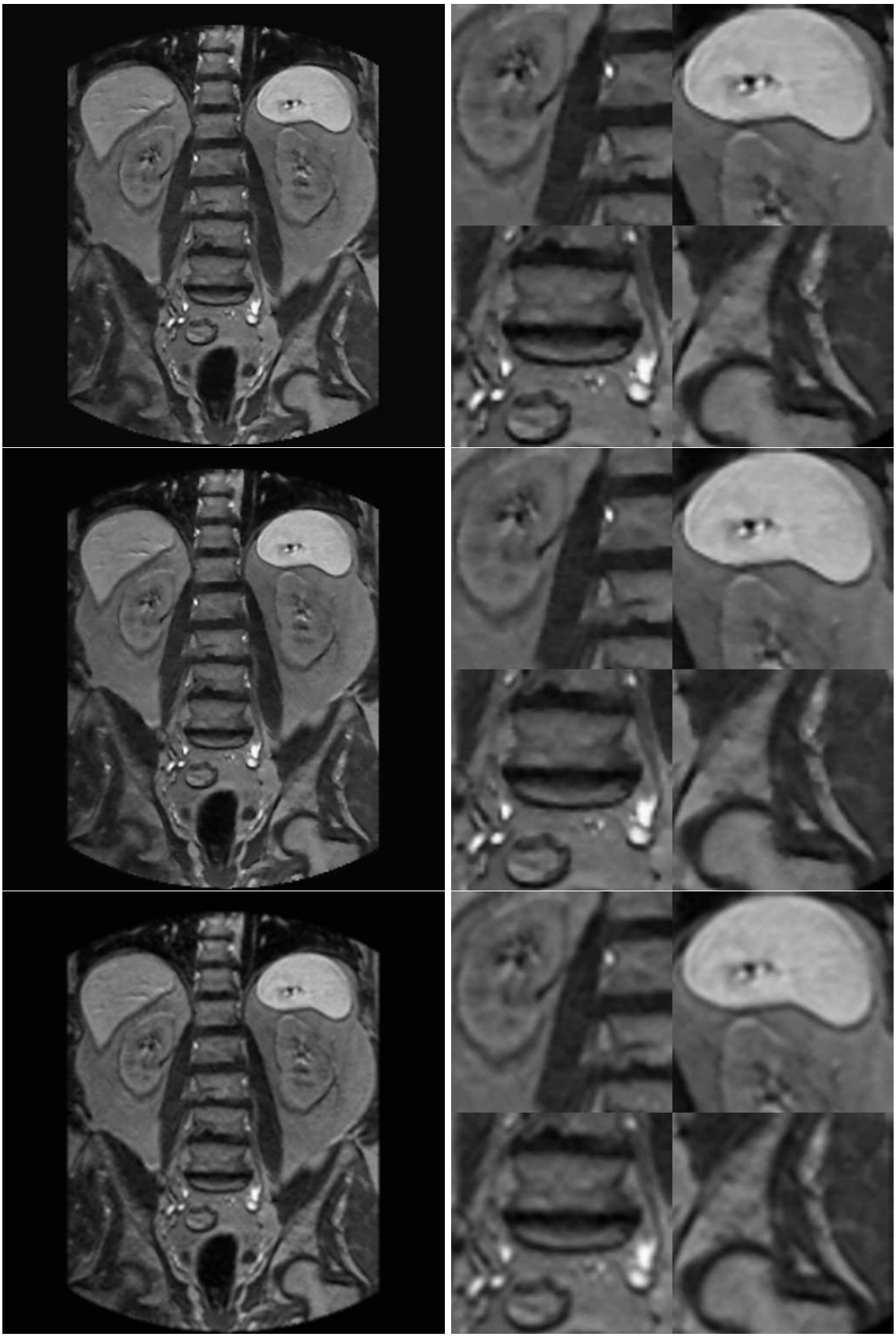

Figure 3: (m) TOP LEFT: u_0 after EFG filtering, (n) MIDDLE LEFT: u_0 after Gauss-TV filtering, (o) BOTTOM LEFT: u_0 after Gauss filtering, and (p – r) RIGHT COLUMN: magnifications from images (m – o), respectively.

Filter	Advantages	Disadvantages
Median	Preserves stronger edges.	Changes the shapes of edges by sawtoothing or by smoothing. Smoothes some details.
BFB	Preserves image details. Can provide multiscale edge enhancement. Is a candidate for segmentation preconditioning.	Creates unnatural image flattening, though less so than PM and TV.
PM	Can enhance a targeted edge strength.	Enhances only a limited range of edge strengths and otherwise edges are either smoothed or staircased. Blurs details and strongly flattens images.
TV	Reduces noise while preserving details.	Staircases regions of gradual variation, and more so with a reaction term. Creates unnatural image flattening.
EFG	Preserves details and avoids staircasing. Is a good candidate for segmentation preconditioning.	Flattens images.
Gauss-TV	Preserves details and avoids staircasing. Preserves natural roundedness of image objects.	Partially preserves some noisy patterns.
Gaussian	Reduces noise.	Preserves some noisy patterns. Isotropic smoothing blurs details.

Table 2: Summary of filter results.

or segmentation preconditioning. Since the filter blurs important details, it is also ill-suited to enhance the visual clarity of medical images.

From Figs. 2c and 2f and Figs. 3c and 3f, it is clear that the BFB filter preserves image details. Also, because of the greater tangential diffusion of the BFB filter, its results are generally smoother than the corresponding TV results. For example, the TV jumps in Figs. 2k and 2l appear as staircasing steps in relation to the more natural corresponding BFB edges in Fig. 2f. The same relation can be observed between the TV filtered spleen images shown in Figs. 3k and 3l and the BFB filtered spleen image shown in Fig. 3f. On the other hand, because of the backward normal diffusion of the BFB filter, its treatment of the flat fluid bath region shown in Figs. 2c and 2f is not as smooth as the corresponding EFG results shown in Figs. 2m and 2p. The associated edge enhancement properties of the BFB filter in relation to the EFG filter are similarly evident in the comparison of Figs. 3c and 3f with Figs. 3m and 3p. Because of the greater staircasing evident in the TV as well as the PM results, the BFB filter appears to be a better tool for segmentation preconditioning. However, because of the smoother results of the EFG filter, its use for segmentation may be more successful than that of the BFB filter. Furthermore, both the EFG filter and the Gauss-TV filter enhance the visual clarity of medical images better than the BFB filter.

As indicated in Section 2, the PM filter enhances edges with gradients inside a narrow range; otherwise, weaker slopes are blurred and stronger slopes are staircased. Specifically, with $\phi''(\lambda) = 0$ and $\phi'''(\chi) = 0$, gradients with $|\nabla u| < \lambda$ are smoothed, gradients with $\lambda < |\nabla u| < \chi = \lambda\sqrt{3}$ are heightened, and gradients with $\chi < |\nabla u|$ are staircased. Consequently, as seen in Figs. 2g, 2j, 3g, and 3j, images are leveled into smoothly shaped flat regions bounded by high contrast edges to which λ happens to be tuned. The resulting characteristic *watercolor* effect is particularly evident in Fig. 2j. The loss of details whose gradients $|\nabla u|$ happen to fall

below the λ threshold is especially apparent in the spleen image in Fig. 3j. Note in Figs. 2g and 2j that the flat fluid bath region is flattened by the PM filter more than any other filter. However, each PM filtered image is, on the whole, unnaturally flattened. As a result, the PM filter is a poor tool for enhancing visual clarity. Nevertheless, the flattening would not be entirely unsatisfactory from the point of view of segmentation preconditioning if the flat region shapes were not so sensitively dependent upon the value of λ. Overall, the PM filter appears also to be a poor tool for segmentation preconditioning.

Concerning the eight images shown for TV filtering, recall from Section 2 that the reaction term in Eqn. (1.2) can contribute to staircasing. In this connection, note that without the reaction term, the TV filtered images in Figs. 2h, 2k, 3h, and 3k, are smoother than their counterparts in Figs. 2i, 2l, 3i, and 3l, which are TV filtered with the reaction term. Nevertheless, with or without the reaction term, TV filtering has reduced noise while preserving details. However, TV filtering clearly flattens an image and creates image jumps, and more so than does BFB filtering but less so than does PM filtering. These comparisons are particularly demonstrated in Figs. 2f, 2j, 2k, and 2l. Also, comparing Figs. 2k and 2l with Fig. 2p demonstrates that EFG filtering treats the flat fluid bath region more smoothly than does TV filtering. In fact, the EFG filtered and the Gauss-TV filtered images are generally more realistic than are the TV filtered images. In sum, the BFB and EFG filters appear to be better suited to segmentation preconditioning than is pure TV filtering, and the EFG and Gauss-TV filters are better suited to visual clarity enhancement than is pure TV filtering.

As indicated earlier, the images shown in Figs. 2m and 2p demonstrate that the EFG filter provides a flatter and yet more natural treatment of the flat fluid bath region than do the other filters. The same trend is demonstrated with respect to the flatter regions in Figs. 3m and 3p, except that these regions are unnaturally flattened by the EFG filter in relation to the Gauss-TV filtered results in Figs. 3n and 3q. Compare Figs. 3p and 3q for example to see the differences in the fat tissue surrounding the kidneys, where the subject's right kidney is shown in the upper left of the figures and the subject's left kidney is shown partly in the upper right. This more realistic three-dimensional appearance seen in the Gauss-TV filtered as opposed to the EFG filtered images can be understood from the fact that, unlike Gauss-TV, the EFG filter approaches the TV filter for ever smaller gradients. On the other hand, both the EFG and Gauss-TV filters treat the finer details more smoothly than do the earlier filters, as demonstrated by comparing the filtered images of the kidneys and vertebra in Fig. 3. Furthermore, this smoother treatment does not appear to have suffered from a significant loss of details. Thus, since the EFG filter flattens images without creating spurious jumps and without smoothing details excessively, it appears to be a very good tool for segmentation preconditioning. Though the Gauss-TV filter better preserves the roundedness of objects instead of flattening them, the EFG filter performs better than the other filters to enhance the visual clarity of medical images.

As explained earlier, the Gauss-TV filter is purely Gaussian for sufficiently small gradients instead of approaching the TV filter like the EFG filter does. As a result, the Gauss-TV filter preserves a realistic roundedness in objects, but also partially preserves the *stippled* noise pattern in flat regions as does the pure Gaussian filter. See especially the results for the flat fluid bath region shown in Figs. 2n, 2q, 2o, and 2r. This accommodation of rounded image features by Gauss filtering can be understood from the variational formulation. Specifically, simple calculations with ℓ_1 and ℓ_2 norms reveal that the TV penalty on $|\nabla u|^1$ permits the local accumulation of large slopes in exchange for a global flatness in u while the Gaussian penalty on $|\nabla u|^2$ seeks a more uniform distribution of slopes instead. Nevertheless, as the Gauss-TV filter is purely TV for sufficiently large gradients, it benefits from the corresponding edge preservation. In fact, the filtered images appearing in Figs. 2n and 2q demonstrate a very good enhancement of visual clarity for a medical image with a very broad range of gradient scales. On the other hand, the performance of the Gauss-TV filter as a segmentation preconditioner, particularly in relation to the EFG filter, must be established by further investigation.

Finally, the Gauss filtered images in Figs. 2o, 2r, 3o, and 3r are obviously isotropically blurred. As mentioned above, the treatment of the flat fluid bath region shown in Figs. 2o and 2r exhibits the *stippled* noise pattern, and more so than with the Gauss-TV filter. Also, as seen in the lower right of Figs. 3q and 3r, the Gaussian filter especially blurs the pointed structures surrounding the subject's left hip, while the TV portion of the Gauss-TV filter provides good edge preservation for these objects. Thus, the Gauss filter is not a good tool for either segmentation preconditioning or for enhancing visual clarity.

5 Conclusions.

Several variational based diffusion filters have been applied to noisy measured magnetic resonance images and evaluated for their suitability to medical imaging. The results can be summarized with the following observations. First, the results reveal that the standard median and Gaussian filters compare poorly with the other filters considered. The median filter strongly changes the shapes of edges either by sawtoothing or by smoothing, and the filter blurs details excessively. The Gaussian filter generates isotropic blurring and thus causes the loss of both fine details and sharp edges. Next, it was found that the BFB, PM, and TV filters lead to unnatural flattening of images, but the BFB filter provides the smoothest results among these filters. Although BFB filter results are less smooth than those of the EFG filter, the BFB filter is a possible candidate for segmentation preconditioning. The PM filter suffers a loss of image details for gradients below a parameter threshold, and thus the filter performs relatively poorly for enhancing visual clarity. Furthermore, the PM filter creates a very strong flattening of images, and since the shapes of flattened regions are strongly parameter dependent, the filter should not be considered an adequate tool for segmentation preconditioning. The TV filter does reduce noise and does preserve details, but also flattens images and creates image jumps. The staircasing effect can also be increased by the presence of the reaction term in the diffusion equation. Clearly the pure TV approach benefits from the modifications introduced in the EFG and Gauss-TV filters. The EFG filter flattens images without creating spurious jumps and without smoothing details excessively. Thus, this filter is a very good candidate for segmentation preconditioning. The Gauss-TV filter preserves the natural roundedness of objects and it preserves edges. As a result, this filter provides very good visual clarity enhancement. Therefore, the total variation based convex EFG and Gauss-TV filters have been demonstrated to perform very well for the goals of medical imaging.

References

[1] N. Nordström, *Biased Anisotropic Diffusion – A Unified Regularization and Diffusion Approach to Edge Detection*, Image Vision Comput., Vol. 8, pp. 318 – 327, 1990.

[2] R. Gonzalez and R. Woods, *Digital Image Processing*, Addison-Wesley, Reading, MA, 1992.

[3] J. Weickert, *Anisotropic Diffusion in Image Processing*, B. G. Teubner Stuttgart, 1998.

[4] S.L. Keeling and R. Stollberger, *Nonlinear Anisotropic Diffusion Filtering for Multiscale Edge Enhancement*, Spezialforschungsbereich F-003 Bericht Nr. 180, Karl-Franzens-Universität Graz, Jännar, 2000 (submitted to *Inverse Problems*).

[5] P. Perona and J. Malik, *Scale Space and Edge Detection Using Anisotropic Diffusion*, Proc. IEEE Comp. Soc. Workshop on Computer Vision, Miami Beach, November 30 – December 2, 1987, IEEE Computer Society Press, Washington, pp. 16 – 22, 1987.

[6] L.I. Rudin, S. Osher, and E. Fatemi, *Total Variation Based Noise Removal Algorithms*, Physica D, Vol. 60, pp. 259 – 269, 1992.

[7] K. Ito and K. Kunisch, *Restoration of Edge-Flat-Grey Scale Images*, Spezialforschungsbereich F-003 Bericht Nr. 161, Karl-Franzens-Universität Graz, Juli, 1999 (to appear in *Inverse Problems*).

[8] C. Schnörr, *Unique Reconstruction of Piecewise-Smooth Images by Minimizing Strictly Convex Nonquadratic Functionals*, J. Math. Imaging and Vision, Vol. 4, pp. 189 - 198, 1994.

[9] S.L. Keeling, R. Bammer, F. Fazekas, and R. Stollberger, *Total Variation Denoising for Improved Diffusion Tensor Calculation*, ISMRM 2000, Denver, CO, April 1-7, 2000.

[10] L. Alvarez, F. Guichard, P.-L. Lions, and J.-M. Morel, *Axioms and Fundamental Equations in Image Processing*, Arch. Rational Mech. Anal., Vol. 123, pp. 199 – 257, 1993.

[11] B. Benhamouda, *Parameter Adaptation for Nonlinear Diffusion in Image Processing*, Master's Thesis, Dept. of Mathematics, University of Kaiserslautern, P.O. Box 3049, 67653 Kaiserslautern, Germany, 1994.

[12] A.N. Tikhonov and V.Y. Arsenin, *Solutions of Ill-Posed Problems*, Wiley, New York, 1977.

[13] C.W. Groetsch, *Inverse Problems in the Mathematical Sciences*, Vieweg, Braunschweig, 1993.

[14] R. Barrett, M.W. Berry, T.F. Chan, J. Demmel, J. Donato, J. Dongarra, V. Eijkhout, R. Pozo, C. Romine, and H. van der Vorst, *Templates for the Solution of Linear Systems: Building Blocks for Iterative Methods*, SIAM, Philadelphia, 1993.